Supplementary Information for

Photoemission Spectroscopy and Microscopy for Ta@Si_{16} Superatom and their Assembled-Layers

Masahiro Shibuta,[‡a] Tsutomu Ohta,[b] Toshiaki Kamoshida,[b] Kana Yamagiwa,[b] Hironori Tsunoyama,[b] Tomoya Inoue,[b] Tsugunosuke Masubuchi,[b] and Atsushi Nakajima*[ab]

[a.] Keio Institute of Pure and Applied Sciences (KiPAS), Keio University, 3-14-1 Hiyoshi, Kohoku-ku, Yokohama 223-8522, Japan

[b.] Department of Chemistry, Faculty of Science and Technology, Keio University, 3-14-1 Hiyoshi, Kohoku-ku, Yokohama 223-8522, Japan

*Address correspondence to A. Nakajima

Tel: +81-45-566-1712, Fax: +81-45-566-1697, E-mail: nakajima@chem.keio.ac.jp

‡ Present address: Department of Physics and Electronics, Graduate School of engineering, Osaka Metropolitan University, 1-1, Gakuen-cho, Naka-ku, Sakai, Osaka 599-8531, Japan.

Table of contents

Note S1. Definition of nominal coverage of Ta@Si_{16} SA. 2
Fig. S1. Coverage dependence of the XPS spectra of Ta@Si_{16} SAs on C_{60} substrate. 3
Fig. S2. XPS spectra for Ta@Si_{16} thick film (7 ML) before and after exposing oxygen. 4
Fig. S3. UPS spectra for Ta@Si_{16} thick film (7 ML) before and after exposing oxygen. 4
Fig. S4. Two-color 2PPE spectra for Ta@Si_{16} SAs on C_{60}. 5
Fig. S5. XPS spectra for Ta@Si_{16} (0.6 ML) deposited on an Au(111) substrate. 5
Fig. S6. Coverage-dependent UPS spectra ($h\nu$ = 21.22 eV) of Ta@Si_{16} SA on C_{60}. 6
Fig. S7. Raw UPS/2PPE spectral data and background subtraction. 6
Note S2. Computational methods. 7
Fig. S8. UPS/2PPE spectra for Ta@Si16 thick film (7 ML) and calculated results. 7
Fig. S9. Optimized structures of cationic and neutral Ta@Si_{16}. 8
Table S1. Eigenvalues of calculated results (eV) for cationic Ta@Si_{16} and their degeneracies. 8
Table S2. Eigenvalues of calculated results (eV) for neutral Ta@Si_{16} and their spins. 10
References 12

Supplementary Note S1. Definition of nominal coverage of $Ta@Si_{16}$ Superatom (SA).

In this note, we estimate the nominal coverage of $Ta@Si_{16}$ SAs. Assuming the size of SA (0.8~0.9 nm in diameter) and the deposition area (6 mmϕ, ca. 2.8×10^{13} nm^2), the amount of deposition for full coverage (monolayer; ML) corresponds to 5×10^{13} SAs. According to the STM result for $Ta@Si_{16}/C_{60}$ at very low coverage (much less than 1 ML),[1,2] individual $Ta@Si_{16}$ SAs are immobilised on the $C_{60}(111)$ surface. It is considered that deposited SAs spread uniformly over the C_{60} surface without self-organization (e.g. island formation) up to full coverage (1 ML). This is because the alkaline-like $Ta@Si_{16}$ SA favorably engages in charge transfer interaction with the n-type organic substrate of C_{60}, which has been discussed in the XPS analysis at a fixed $Ta@Si_{16}$ SA coverage (0.6 ML).[3-7] After completing the ML, it is considered that the $Ta@Si_{16}$ SA film grows on the ML surface in a quasi-layer-by-layer growth manner. The above coverage definition and growth manner of the SA film are justified by the step-by-step measurement of XPS spectra.

Supplementary Fig. S1 (a)-(c) shows XPS spectra around the (a) Si 2p, (b) Ta 4f, and (c) C 1s core levels at various deposition amounts ($0 - 35 \times 10^{13}$ clusters, denoted in the right) of $Ta@Si_{16}$ SAs on a C_{60} substrate. Both core levels of Ta 4f and Si 2p are clearly resolved by the $Ta@Si_{16}$ deposition. At the initial deposition (1.4×10^{13} Clusters), the intensity ratio between the Ta 4f and Si 2p core levels is consistent with the atomic composition ratio of 1 : 16 for $Ta@Si_{16}$ SA.[3,4] Furthermore, the XPS peaks of Si 2p and Ta 4f are well-reproduced by considering uniform chemical components within the experimental peak broadening, which demonstrates the successful immobilisation of $Ta@Si_{16}$ on the C_{60} substrate while preserving its caged structure.

At higher amounts of $Ta@Si_{16}$ SA deposition of more than 5×10^{13} SAs (i.e., > 1 ML, the intensity ratios, peak widths, and energies remain mostly the same at any deposition amount, suggesting that the SA film formed on the first $Ta@Si_{16}$ layer, preserving the chemical composition and geometric structure of the SA. The intensities of the Si 2p- and Ta 4f-derived peaks increase with the deposition amount, whereas the XPS intensity of the C 1s peak originating from C_{60} substrate (Fig. 2 (c)) decreases with SA

deposition at higher coverages, and is mostly quenched at the highest coverage (35 × 10^{13} SAs) because of the overlayered SA film. The decrease in the C 1s signal intensity with increasing the deposition amount is associated with uniform assembly of SAs on the substrate; otherwise (e.g. 3D growth), the XPS signal from substrates should remain even at higher coverage. From these results, it can be concluded that the Ta@Si_{16} film grows on an organic substrate in a quasi-layer-by-layer growth manner.

The C 1s peak in Fig. S1(c) shifts slightly towards higher binding energy with increasing Ta@Si_{16} coverage up to ~5 × 10^{13} SAs (1 ML), which can be explained by the charge transfer interaction between Ta@Si_{16} SA and C_{60} molecule.[4] The saturation of the C 1s peak shift justifies the abovementioned ML definition estimated by the amount of the SA deposition into a deposition area (6 mmϕ), namely, 1 ML ≈ 5 × 10^{13} SAs, because further deposition on the 1 ML Ta@Si_{16} film does not affect the charge state of underlying C_{60}.

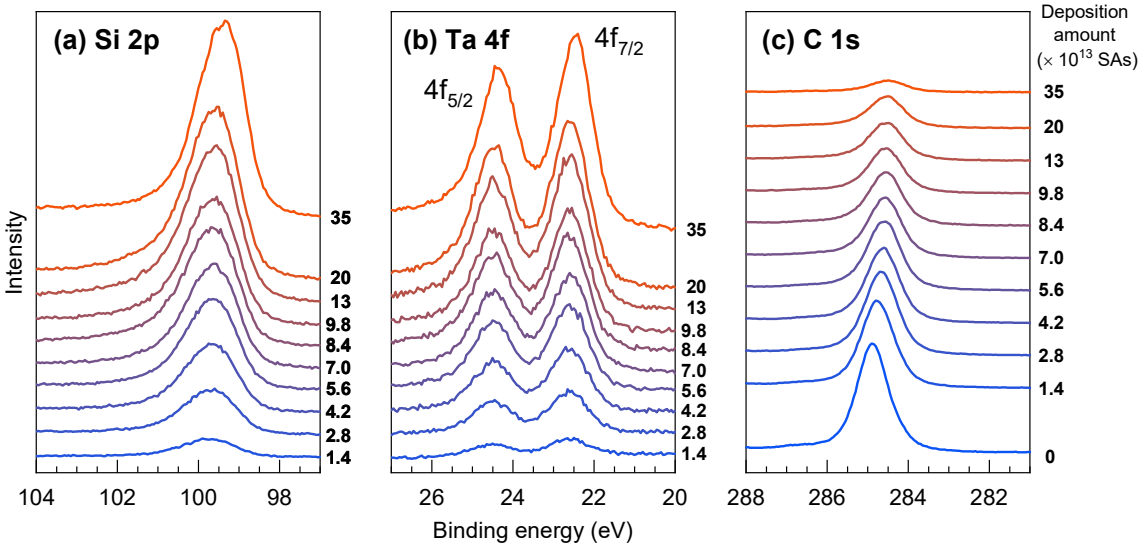

Supplementary Fig. S1. Coverage dependence of the XPS spectra of Ta@Si_{16} SAs on C_{60} substrate. The XPS spectra are near the (a) Si 2p, (b) Ta 4f, and (c) C 1s core levels. The deposition amounts, in units of 10^{13} SAs, are presented on the right side of each figure. Both Ta 4f and Si 2p peaks increase with SA coverage, while their widths can be reproduced by single chemical components.[3,4] The C 1s signal is attenuated by SA deposition, suggesting the formation of a uniform Ta@Si_{16} SA film on the C_{60} substrate.

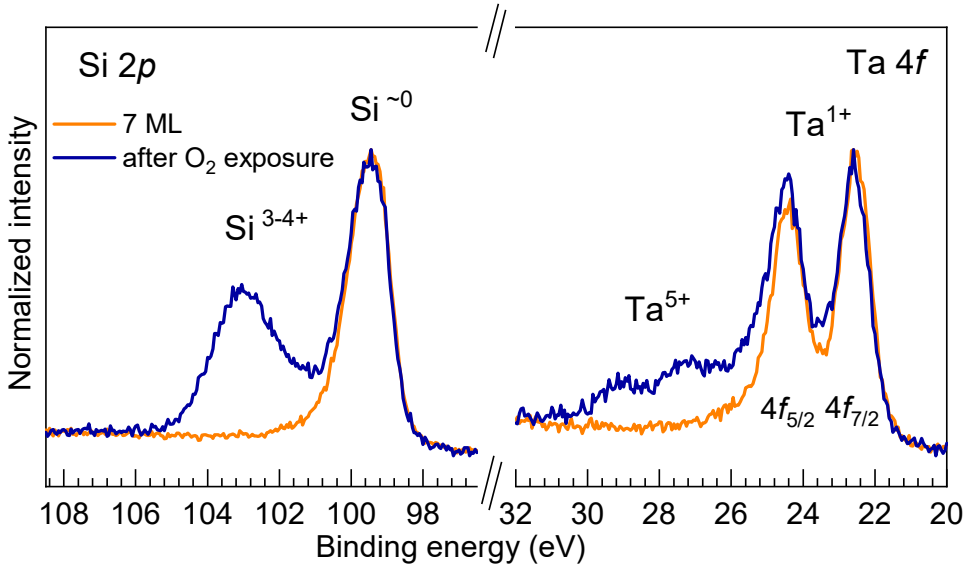

Supplementary Fig. S2. XPS spectra for Ta@Si$_{16}$ thick film (7 ML) before and after exposing oxygen (1atm for 40 hours). The Si 2p derived peak shows Si^{3-4+}-derived chemical components owing to the oxidation of the Ta@Si_{16}. Ta atom is also oxidized in part, while it is rather robust toward oxidative reaction because of the metal encapsulation.

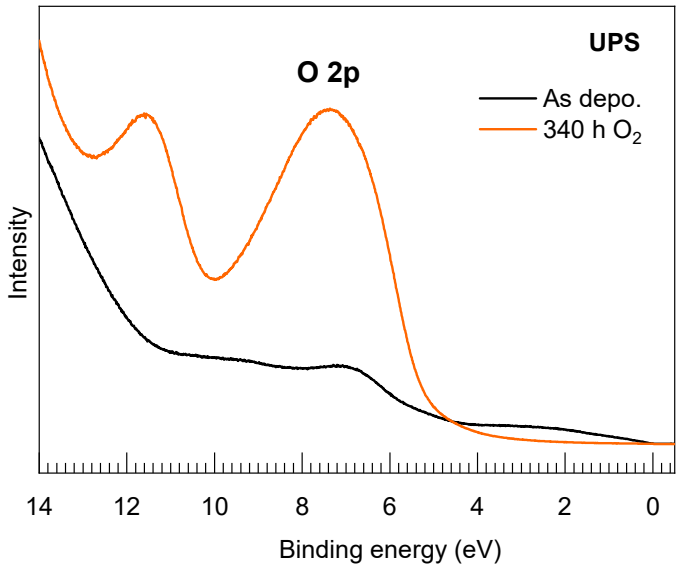

Supplementary Fig. S3. UPS spectra (raw data) for Ta@Si$_{16}$ thick film (7 ML) before and after exposing oxygen (1atm for 40 hours). After O_2 exposures, strong O 2p derived feature is observed at the biding energy of 7 eV, showing the oxidative reaction of Ta@Si_{16} SAs. UPS is more sensitive to the surface oxidations rather than that for the XPS (Fig. S2) because of the shorter mean-free-path of photoelectrons.

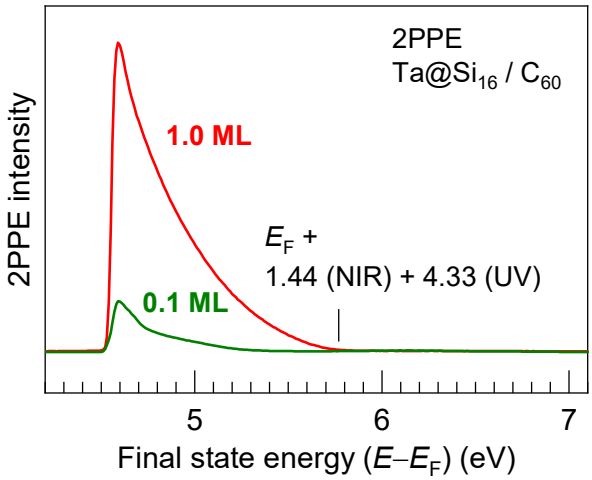

Supplementary Fig. S4. Two-color 2PPE spectra for Ta@Si_{16} SAs on C_{60}. The photon energies of the NIR and UV lasers are 1.44 eV and 4.33 eV, respectively. The 2PPE intensity below the Fermi edge (1.44 eV + 4.33 eV in the final state energy) is enhanced by the SA deposition. It is important to note that no measurable photoemission is detected in the absence of SA deposition.

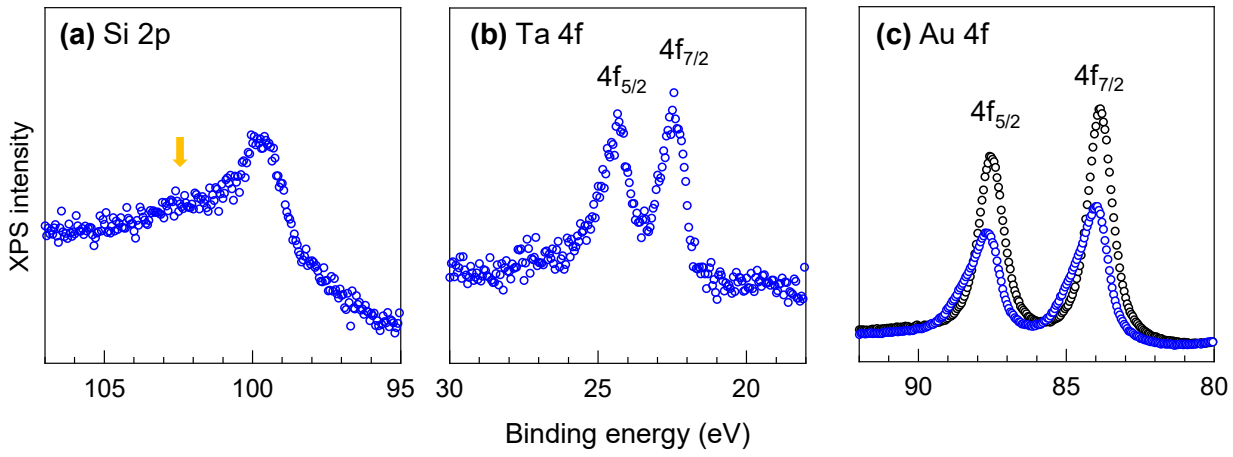

Supplementary Fig. S5. XPS spectra for Ta@Si_{16} (0.6 ML) deposited on an Au(111) substrate. (a) Si 2p, (b) Ta 4f, and (c) Au 4f core levels. Si 2p derived peak shows multiple chemical components (vertical arrow), suggesting that the deposited Ta@Si_{16} SA is chemically affected by the interaction with Au (111) substrate. The Au 4f peaks also differ from that of a clean Au substrate, showing the chemical modification of Au side by the deposition of Ta@Si_{16} SAs.

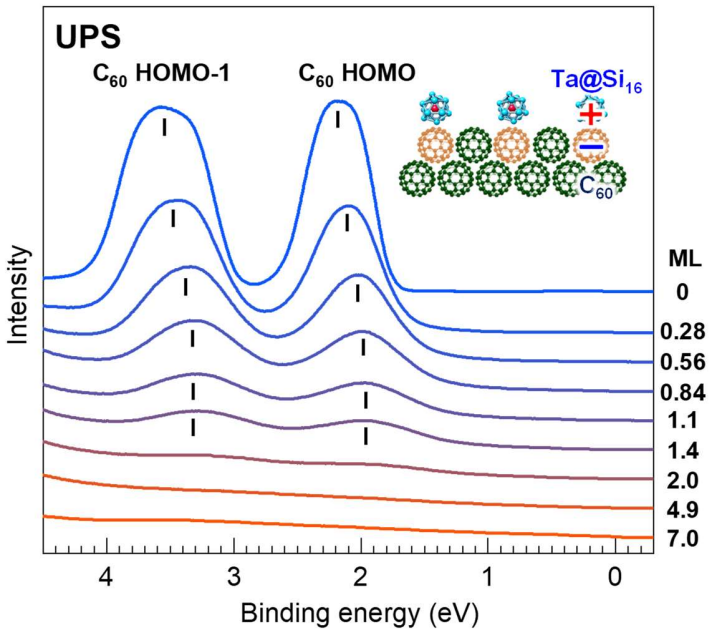

Supplementary Fig. S6. Coverage-dependent UPS spectra ($h\nu$ = 21.22 eV) of Ta@Si_{16} SA on C_{60}. The C_{60}-derived HOMO and HOMO-1 peaks are attenuated by SA deposition up to 7 ML, with a slight upshift of 0.2 eV, suggesting that a charge transfer interaction occurs between SA and C_{60} at the interface. The C_{60}-derived features completely disappear in multilayered SA films thicker than 2 ML, indicating that fully covered SA films are formed. The inset shows a schematic illustration of the charge transfer complexation of Ta@Si_{16} SAs with C_{60} molecules.

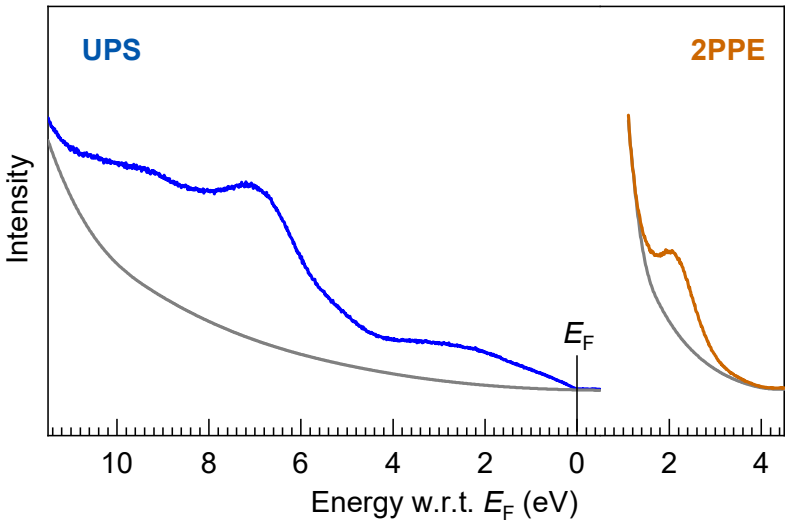

Supplementary Fig. S7. Raw UPS/2PPE spectral data and background subtraction. Appropriate backgrounds (grey) with spline curves are subtracted from raw data of UPS and 2PPE spectra (colored spectra).

Note S2. Computational methods.

The electronic structures of optimized Ta@Si_{16} neutrals and cations were calculated using the Gaussian 09 (cations)[8] and Gaussian 16 (neutrals)[9] programs, at several different levels of the density functional theory. The Ahlrichs' basis sets def-TZVP (for cations)[10] or def2-TZVP (for neutrals) were utilized for Si and Ta. For Ta, a 60-electron relativistic effective core potential was also employed. The hybrid exchange-correlation functional of B3LYP[11] and pure functional of PBEPBE,[12] and hybrid PBE0 functional[13] and Slater-type TZ2P basis-set[14] were utilized. These calculations were carried out for the optimized structures of cationic M@Si_{16} isomers at the PBEPBE/def-TZVP level (Gaussian 09). The details of the coordinates are described elsewhere.[15]

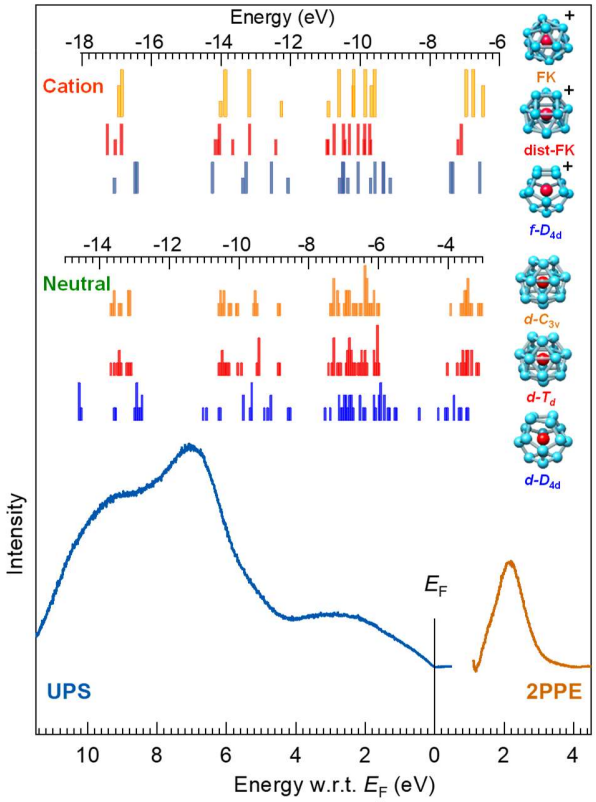

Supplementary Fig. S8. UPS, 2PPE, and calculated results. (bottom) UPS and 2PPE spectra of a thick Ta@Si_{16} SA film (7 ML). The energy onset at E_F in the UPS spectrum indicates Ohmic electronic conduction of the Ta@Si_{16} SA film. The broad valence and conduction band features at E_F – 2.6 eV, – 7.0 eV, and – 9.6 eV in UPS and at E_F + 2.1 eV in 2PPE are observed. (upper) Calculated energy levels of free Ta@Si_{16} SAs in a cationic state (top three) and in a neutral state (lower three) for optimized isomeric structures, where the total energies in each charge state vary minimally among the three structures (see also Fig. S9): Frank-Kasper (FK), distorted FK, and *f*-D_{4d} for cations, and *d*-C_{3V}, *d*-T_d, and *f*-D_{4d} for neutrals, as shown in the right part of the figure. The energy levels align moderately with the experimental observations (lower spectra), whereas the energies of unoccupied levels are underestimated in the present calculations.

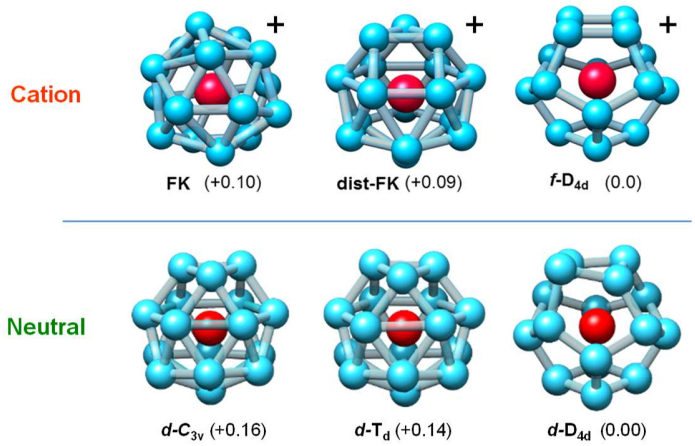

Supplementary Fig. S9. Optimized structures of cationic and neutral Ta@Si$_{16}$. The symmetries and energies relative to the most stable isomer (in eV) are indicated at the bottom of each structure.

Supplementary Table S1. Eigenvalues of calculated results (eV) for neutral Ta@Si$_{16}$ and their degeneracies. The values in blue and red correspond to HOMO and LUMO levels, respectively.

FK	Degen.	Dist.-FK	Degen.	*f*-D_{4d}	Degen.
-20.70	1	-20.71	1	-19.80	1
-18.98	3	-19.05	2	-18.67	1
-16.97	2	-18.80	1	-18.09	2
-16.89	3	-17.14	2	-17.02	1
-14.05	1	-16.91	1	-16.42	2
-13.92	3	-16.73	2	-16.38	2
-13.23	3	-14.03	1	-14.20	2
-12.31	1	-13.96	1	-13.33	1
-10.95	1	-13.91	2	-13.23	2
-10.65	3	-13.53	1	-12.51	2
-10.24	2	-13.05	2	-12.03	1
-10.23	3	-12.30	1	-10.54	1
-9.90	3	-10.82	1	-10.47	1
-9.72	2	-10.80	1	-10.46	2
-9.63	**3**	-10.62	2	-10.44	2
-6.99	**3**	-10.35	2	-10.31	1
-6.78	3	-10.32	1	-10.01	2
-6.51	2	-10.18	2	-9.65	1
-5.70	3	-9.92	2	-9.53	2
-5.70	1	-9.76	1	-9.29	2
-5.42	3	-9.74	2	-9.28	2
-4.05	3	-9.59	2	**-9.09**	**1**
-3.96	2	**-9.57**	**1**	**-7.35**	**2**
-3.94	1	**-7.06**	**1**	-7.30	2
-3.63	3	-6.96	2	-6.52	2
		-6.94	1	-5.66	2
		-6.89	2	-5.36	1

-6.50	2	-5.28	2
-5.81	2	-4.98	1
-5.75	1	-4.95	2
-5.46	2	-4.49	1
-5.39	1	-4.48	2
-5.13	1	-4.11	1
-4.29	2	-3.82	1
-4.07	1	-3.60	1
-3.98	1	-3.46	2
-3.86	2	-2.80	2
-3.56	1	-2.65	2
-3.45	2		

Supplementary Table S2. Eigenvalues of calculated results (eV) for neutral Ta@Si_{16} and their spin orbitals. The values in blue and red correspond to HOMO and LUMO levels, respectively.

d-D_{4d}	Spin	*d*-T_d	Spin	*d*-C_{3v}	Spin
-14.58	α	-13.66	α	-13.65	α
-14.57	α	-13.60	β	-13.61	α
-14.56	β	-13.46	α	-13.60	β
-14.54	β	-13.44	α	-13.57	β
-13.59	α	-13.41	β	-13.42	α
-13.55	β	-13.39	β	-13.37	β
-12.99	α	-13.24	α	-13.18	α
-12.94	α	-13.18	β	-13.15	α
-12.93	β	-13.11	α	-13.13	β
-12.92	β	-13.09	β	-13.12	β
-12.85	α	-10.59	α	-10.56	α
-12.81	β	-10.53	α	-10.51	α
-12.79	α	-10.49	β	-10.50	β
-12.76	β	-10.46	β	-10.47	α
-11.04	α	-10.42	α	-10.42	β
-10.94	β	-10.37	β	-10.40	β
-10.56	α	-10.32	α	-10.27	α
-10.52	β	-10.27	β	-10.23	β
-9.88	α	-10.01	α	-10.06	α
-9.86	β	-9.94	β	-10.00	β
-9.70	α	-9.49	α	-9.56	α
-9.65	β	-9.44	β	-9.54	α
-9.64	α	-9.44	α	-9.53	β
-9.62	β	-9.41	β	-9.49	β
-9.26	α	-8.88	α	-8.87	α
-9.16	β	-8.83	β	-8.82	β
-9.08	α	-7.41	α	-7.37	α
-9.07	β	-7.33	α	-7.32	α
-8.55	α	-7.27	β	-7.29	β
-8.51	β	-7.26	β	-7.26	β
-7.55	α	-7.25	α	-7.26	α
-7.36	β	-7.18	β	-7.17	β
-7.14	α	-7.14	α	-7.17	α
-7.11	α	-7.10	β	-7.14	β
-7.09	β	-6.94	α	-6.97	α
-7.05	β	-6.88	β	-6.92	α
-6.99	α	-6.87	α	-6.92	α
-6.97	β	-6.84	α	-6.87	β
-6.94	α	-6.83	α	-6.87	β
-6.91	β	-6.82	β	-6.83	β
-6.86	α	-6.78	β	-6.80	α
-6.83	β	-6.77	β	-6.72	β
-6.81	α	-6.70	α	-6.66	α
-6.78	β	-6.67	β	-6.64	β
-6.78	α	-6.58	α	-6.54	α

-6.70	β	-6.51	β	-6.48	β
-6.55	α	-6.49	α	-6.40	α
-6.53	β	-6.45	β	-6.40	α
-6.45	α	-6.42	α	-6.36	α
-6.37	β	-6.36	α	-6.36	β
-6.13	α	-6.35	β	-6.32	β
-6.11	β	-6.32	β	-6.32	α
-6.06	α	-6.13	α	-6.31	β
-5.98	α	-6.10	β	-6.28	β
-5.97	β	-6.09	α	-6.20	α
-5.93	α	-6.05	α	-6.17	β
-5.92	β	-6.04	β	-6.15	α
-5.91	β	-6.02	β	-6.11	β
-5.84	α	-6.01	α	-6.02	α
-5.81	β	-5.97	β	-5.97	β
-5.72	α	**-4.01**	**α**	**-3.93**	**α**
-5.68	β	**-3.71**	**β**	**-3.63**	**β**
-5.52	α	-3.60	α	-3.55	α
-5.48	β	-3.58	α	-3.51	α
-4.82	**α**	-3.57	β	-3.51	β
-4.29	**β**	-3.55	β	-3.48	β
-4.08	α	-3.50	α	-3.46	α
-4.04	β	-3.46	α	-3.44	α
-3.83	α	-3.45	β	-3.42	β
-3.81	β	-3.40	β	-3.41	β
-3.67	α	-3.35	α	-3.36	α
-3.61	β				
-3.48	α				
-3.43	β				
-2.91	α				

References

1. M. Nakaya, T. Iwasa, H. Tsunoyama, T. Eguchi and A. Nakajima, *Nanoscale*, 2014, **6**, 14702–14707.
2. M. Nakaya, T. Iwasa, H. Tsunoyama, T. Eguchi and A. Nakajima, *J. Phys. Chem. C*, 2015, **119**, 10962–10968.
3. M. Shibuta, T. Ohta, M. Nakaya, H. Tsunoyama, T. Eguchi and A. Nakajima, *J. Am. Chem. Soc.*, 2015, **137**, 14015–14018.
4. T. Ohta, M. Shibuta, H. Tsunoyama, T. Eguchi and A. Nakajima, *J. Phys. Chem. C*, 2016, **120**, 15265–15271.
5. M. Shibuta, T. Kamoshida, T. Ohta, H. Tsunoyama and A. Nakajima, *Commun. Chem*., 2018, **1**, 50.
6. T. Kamoshida, M. Shibuta, T. Ohta, T. Eguchi and A. Nakajima, *J. Phys. Chem. C*, 2022, **126**, 10889–10899.
7. K. Terasaka, T. Kamoshida, T. Ichikawa, T. Yokoyama, M. Shibuta and A. Nakajima, *J. Am. Chem. Soc.*, 2024, **146**, 9605–9613.
8. Gaussian 09, Revision E.01, M. J. Frisch, G. W. Trucks, H. B. Schlegel, G. E. Scuseria, M. A. Robb, J. R. Cheeseman, G. Scalmani, V. Barone, B. Mennucci, G. A. Petersson, H. Nakatsuji, M. Caricato, X. Li, H. P. Hratchian, A. F. Izmaylov, J. Bloino, G. Zheng, J. L. Sonnenberg, M. Hada, M. Ehara, K. Toyota, R. Fukuda, J. Hasegawa, M. Ishida, T. Nakajima, Y. Honda, O. Kitao, H. Nakai, T. Vreven, J. A. Montgomery, Jr., J. E. Peralta, F. Ogliaro, M. Bearpark, J. J. Heyd, E. Brothers, K. N. Kudin, V. N. Staroverov, R. Kobayashi, J. Normand, K. Raghavachari, A. Rendell, J. C. Burant, S. S. Iyengar, J. Tomasi, M. Cossi, N. Rega, J. M. Millam, M. Klene, J. E. Knox, J. B. Cross, V. Bakken, C. Adamo, J. Jaramillo, R. Gomperts, R. E. Stratmann, O. Yazyev, A. J. Austin, R. Cammi, C. Pomelli, J. W. Ochterski, R. L. Martin, K. Morokuma, V. G. Zakrzewski, G. A. Voth, P. Salvador, J. J. Dannenberg, S. Dapprich, A. D. Daniels, Ö. Farkas, J. B. Foresman, J. V. Ortiz, J. Cioslowski, and D. J. Fox, Gaussian, Inc., Wallingford CT, 2013.
9. Gaussian 16, Revision C.01, M. J. Frisch, G. W. Trucks, H. B. Schlegel, G. E. Scuseria, M. A. Robb, J. R. Cheeseman, G. Scalmani, V. Barone, G. A. Petersson, H. Nakatsuji, X. Li, M. Caricato, A. V. Marenich, J. Bloino, B. G. Janesko, R. Gomperts, B. Mennucci, H. P. Hratchian, J. V. Ortiz, A. F. Izmaylov, J. L. Sonnenberg, D. Williams-Young, F. Ding, F. Lipparini, F. Egidi, J. Goings, B. Peng, A. Petrone, T. Henderson, D. Ranasinghe, V. G. Zakrzewski, J. Gao, N. Rega, G. Zheng, W. Liang, M. Hada, M. Ehara, K. Toyota, R. Fukuda, J. Hasegawa, M. Ishida, T. Nakajima, Y. Honda, O. Kitao, H. Nakai, T. Vreven, K. Throssell, J. A. Montgomery, Jr., J. E. Peralta, F. Ogliaro, M. J. Bearpark, J. J. Heyd, E. N. Brothers, K. N. Kudin, V. N. Staroverov, T. A. Keith, R. Kobayashi, J. Normand, K. Raghavachari, A. P. Rendell, J. C. Burant, S. S. Iyengar, J. Tomasi, M. Cossi, J. M. Millam, M. Klene, C. Adamo, R. Cammi, J. W. Ochterski, R. L. Martin, K. Morokuma, O. Farkas, J. B. Foresman, and D. J. Fox, Gaussian, Inc., Wallingford CT, 2019.
10. A. Schäfer, H. Horn and R. Ahlrichs, *J. Chem. Phys*., 1994, **100**, 5829−5835.
11. C. Lee, W. Yang and R. G. Parr, *Phys. Rev. B: Condens. Matter Mater. Phys*., 1988, **37**, 785−789.
12. J. P. Perdew, K. Burke and M. Ernzerhof, *Phys. Rev. Lett*., 1996, **77**, 3865−3868.
13. M. Ernzerhof and G. E. Scuseria, *J. Chem. Phys*.,1999, **110**, 5029−5036.
14. E. van Lenthe and E. J. Baerends, *J. Comput. Chem*., 2003, **24**, 1142−1156.
15. T. Inoue, T. Ina, H. Masai, N. Kondo, F. Matsui, T. Kinoshita and A. Nakajima, *J. Phys. Chem. Lett*. 2024, **15**, 5376–5381.